Ionospheric symmetry caused by geomagnetic declination over North America

Shun-Rong Zhang,[1] Ziwei Chen,[1,2] Anthea J. Coster,[1]
Philip J. Erickson,[1] and John C. Foster[1]

Received 6 September 2013; revised 4 October 2013; accepted 7 October 2013.

[1] We describe variations in total electron content (TEC) in the North American sector exhibiting pronounced longitudinal progression and symmetry with respect to zero magnetic declination. Patterns were uncovered by applying an empirical orthogonal function (EOF) decomposition procedure to a 12 year ground-based American longitude sector GPS TEC data set. The first EOF mode describes overall average TEC, while the strong influence of geomagnetic declination on the midlatitude ionosphere is found in the second EOF mode (or the second most significant component). We find a high degree of correlation between spatial variations in the second EOF mode and vertical drifts driven by thermospheric zonal winds, along with well-organized temporal variation. Results strongly suggest a causative mechanism involving varying declination with longitude along with varying zonal wind climatology with local time, season, and solar cycle. This study highlights the efficiency and key role played by the geomagnetic field effect in influencing mesoscale ionospheric structures over a broad midlatitude range. **Citation:** Zhang, S.-R., Z. Chen, A. J. Coster, P. J. Erickson, and J. C. Foster (2013), Ionospheric symmetry caused by geomagnetic declination over North America, *Geophys. Res. Lett.*, *40*, doi:10.1002/2013GL057933.

1. Introduction

[2] Large spatial variations of the upper atmosphere have often been explained in terms of the offset between magnetic and geographic coordinates [*Rishbeth*, 1998; *Zeng et al.*, 2008]. In this study, we will for the first time visualize observations of detailed mesoscale ionospheric structures clearly suggesting the fundamental influence of magnetic declination, through an analysis of total electron content (TEC) long-term measurements over North America where a dense network of GPS receivers exist.

[3] Geomagnetic declination varies over the globe, with zones of positive and negative declinations occurring alternatively; in North America, the zero declination line is along 85°W–95°W longitudes. In sectors of significant declination change, midlatitude ionospheric variations can be significantly affected by a dynamic process combining declination controls with thermospheric zonal wind influences. This process is a contributing factor to some nighttime ionospheric variations [e.g., *Kil et al.*, 2006; *Luan et al.*, 2008; *He et al.*, 2011] and to the Weddell Sea anomaly, characterized as an electron density-evening enhancement in summer [*Lin et al.*, 2010; *de Larquier et al.*, 2011].

[4] Recently, the community has identified a new class of ionospheric longitudinal variations at midlatitudes across zero magnetic declination. These variations exhibit east-west electron density differences with characteristic diurnal and seasonal variations. They were first noticed over the U.S. continent [*Zhang et al.*, 2011] and then confirmed through statistical analysis in the North and South American and Oceania sectors [*Xu et al.*, 2013]. Comparisons between American and Asian sectors also revealed significant east-west differences with varying characteristics depending on geophysical conditions [*Zhao et al.*, 2013]. A declination-zonal wind mechanism was proposed to account for this class of variations based on long-term observations by the Millstone Hill midlatitude incoherent scatter radar in the northeast U.S. [*Zhang et al.*, 2012a] and by collocated Fabry-Perot interferometer (FPI) observations. Correlation between incoherent scatter radar-derived east-west density differences at night and FPI thermospheric zonal winds is very strong, exceeding 0.95 [*Zhang et al.*, 2012b]. Sporadic reports for similar east-west differences observed over paired stations and speculative suggestions for the declination control and neutral wind contributions have been available in the literature since 1960s [*Eyfrig*, 1963; *Goldberg*, 1966; *Kohl et al.*, 1969].

[5] Given the fact that key ionospheric drivers such as meridional winds are likely not distributed uniformly with longitude, east-west ionospheric differences driven by significant zonal wind-declination effects have often been postulated, but more observational based studies of these effects are needed. In this study, we focus on the questions of whether these postulated east-west differences are statistically significant in space and time and whether these differences fit the more general picture of longitudinal ionospheric variation which follows a gradual longitudinal change of declination. Our study reveals that these effects are indeed present and significant. In particular, a very symmetric longitudinal variation in TEC with respect to the zero declination line stands out markedly using an empirical orthogonal function (EOF) decomposition analysis on a GPS TEC data set spanning more than a full solar cycle in 2001–2012. This EOF approach allows for separation of spatial and temporal variations and provides a basis set of components with varying significances along with an ordered hierarchy of modes. We find that this analysis provides a geophysically meaningful way of investigating a large observational data set.

[1]Haystack Observatory, Massachusetts Institute of Technology, Westford, Massachusetts, USA.
[2]Institute of Electronics, Chinese Academy of Sciences, Beijing, China.

Corresponding author: Shun-Rong Zhang, Haystack Observatory, Massachusetts Institute of Technology, Off Route 40, Westford, MA 01886, USA. (shunrong@haystack.mit.edu)

0094-8276/13/10.1002/2013GL057933

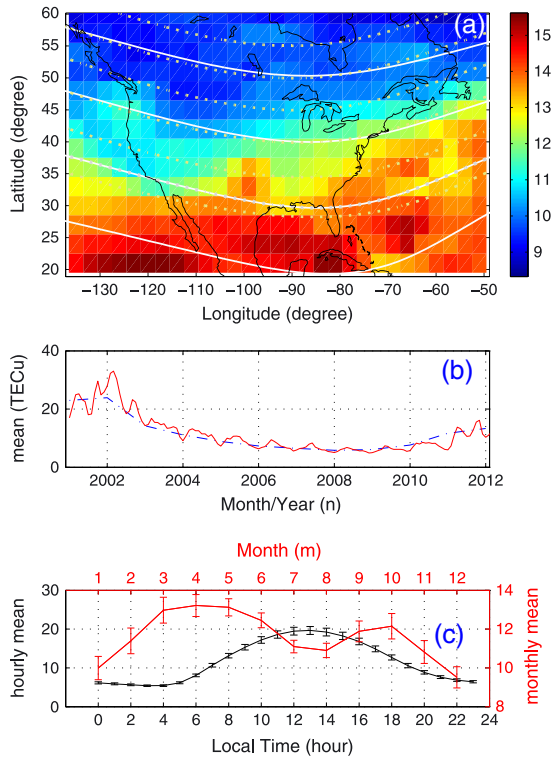

Figure 1. GPS TEC variations over North America averaged over the entire data set. (a) Spatial variation averaged over all times. Superposed are the contours of CGM magnetic latitudes (white solid line) and of meridional wind (200 m/s) induced vertical drifts $v_{\perp}^{m} = 200 \cos I \sin I \cos D$ (dotted lines). (b) Yearly (dash-dotted blue line) and monthly (solid red line) variation averaged over local times, latitudes, and longitudes. (c) Seasonal (monthly) and local time variations, averaged over different latitudes and longitudes as well as over local times or over months. Error bars represent standard deviations.

2. Data and Methodology

2.1. Data

[6] Our study uses GPS TEC data for our variation analysis. The Massachusetts Institute of Technology (MIT) Automated Processing of GPS (MAPGPS) system generates and archives global TEC data in bins of 1° (latitude) × 1° (longitude) at 5 min cadence. The TEC data are derived from worldwide GPS observations [*Mannucci et al.*, 1998; *Coster et al.*, 2003]. Satellite biases are provided by Jet Propulsion Laboratory and receiver biases are estimated [*Rideout and Coster*, 2006]. GPS satellite biases that are used have been shown to be consistent on a monthly basis [*Wilson et al.*, 1999]. MAPGPS tracks closely errors from measurements and data processing. The current study will focus on continuous observations made during 2001–2012 over North America within the geodetic coordinate range (20°N–60°N, 135°W–50°W).

[7] The daily TEC is first binned into hourly bins of 3°× 3° latitude and longitude resolution and then bin averages of the TEC are calculated. Following this, monthly means are derived for each local time and latitude and longitude bin. Since we are interested in quiet time behavior, data with Kp≥3 are excluded. Notice that in the original data, there are very small but persistent offshore data gaps, mostly near the lowest latitudes of east-most and west-most edges. The decomposition step which follows requires a uniform data set with continuous coverage in space and time; therefore, these gaps are filled with data from a Kriging interpolation. This statistics-based linear estimator makes use of surrounding measurements to derive unbiased optimal values for missing points, with appropriate error estimates. These measurements are weighted based on the distance between locations of measurements and data gaps and the overall spatial distribution of the measurements [*Orus et al.*, 2005].

[8] Following this initial binning and averaging, we obtain hourly data for each month which can be analyzed for general TEC characteristics. Figure 1a shows spatial TEC variation, and Figure 1b shows temporal TEC variation. When spatial variations are averaged over all times for each given locations, we find a gradual increase in TEC toward lower geographic latitudes along with some longitudinal dependence. All these suggest modification by effects keyed to magnetic latitude (white solid lines). Figure 1b gives monthly and yearly variations, obtained with averaging over local times and locations. Unsurprisingly, yearly variations track solar cycle phase (see Figure 3b for variations in a solar activity proxy). Figure 1c shows detailed seasonal and local time variations over the entire region averaged over the 12 year period analyzed. Semiannual peaks are found in equinoxes near April and October, with the spring equinox being higher in TEC. Summer TEC levels are close to winter TEC levels and in some cases exceed them. The diurnal maximum appears at 13:00 LT. We use these statistical characteristics (which on their own are of potential interest to other climatology studies) [*Rishbeth*, 1998; *Lei et al.*, 2012; *Qian et al.*, 2013] to set background and first-order ionospheric conditions and proceed in the following sections to examine smaller-scale variations.

2.2. EOF Decomposition

[9] To perform empirical orthogonal function (EOF) decomposition, 2-D hourly (t) and monthly (n, months throughout the 12 years) TEC values T can be expressed mathematically by a set of orthogonal basis functions $b(\phi, \lambda)$ in latitude (λ) and longitude (ϕ). These basis functions are determined from the data set itself rather than by predefined functions,through construction of corresponding principal components $P(t, n)$ with an explicit temporal variation, i.e., $T(t, n, \phi, \lambda) = \sum_{i=1}^{I} b_i(\phi, \lambda) P_i(t, n)$, where $i = 1, ..., I$ represents a series of modes. The EOF approach determines the most likely basis function set b_i by computing the eigenvectors of the covariance matrix $\mathbf{C}$ for the data $T(t, n, \phi, \lambda)$, along with eigenvalues ω_i in the equation $\mathbf{C}\mathbf{b}_i = \omega_i \mathbf{b}_i$. Resulting EOF basis functions b_i are ordered in importance by the magnitude of ω_i for each function. Depending on geophysical processes, the first four modes may account for >97% variance in the data, as is the case in this study and others [*Zhao et al.*, 2005; *A et al.*, 2012; *Lei et al.*, 2012]. The powerful EOF decomposition technique has found a number of recent applications to upper atmospheric modeling and data analysis; *Daniell Jr. et al.* [1995] and *Matsuo et al.* [2002] are examples of earlier attempts on large ionospheric data sets.

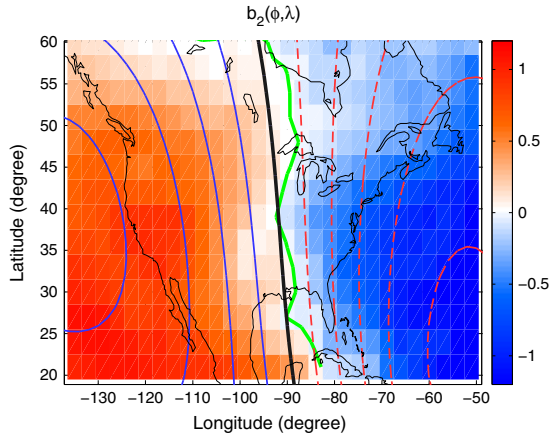

Figure 2. Basis function $b_2(\phi, \lambda)$ for the second EOF mode (see text) derived from EOF decomposition, indicating strong longitudinal dependence controlled by magnetic declination. We note that $b_2(\phi, \lambda)$ is either positive or negative, depending on longitude, with zero values along the longitudes marked by the white area and the green curve. The zero magnetic declination is along the black line. Solid blue lines (+) and dashed red lines (–) mark contours of the quantity $v_\perp^z = 200 \cos I \sin I \sin D$ at intervals of five units, highlighting declination (D) and dip (I) angle effects.

3. Result: TEC Variations in Mode 2

[10] EOF decomposition separates spatial and temporal variations of various modes and assigns them different relative strengths. The most significant variation is contained in the first EOF mode, which accounts for ~94% of the variance in the data. This mode is essentially equivalent to the overall averages as discussed in the previous section and shown in Figure 1. They exhibit a primary latitudinal variation with clear modification by background magnetic field geometry. We call attention to the large and significant second EOF mode in Figures 2 and 3.

3.1. Spatial Variations $b_2(\phi, \lambda)$

[11] The EOF basis function for the second mode, $b_2(\phi, \lambda)$, has a clear longitudinal dependence (Figure 2). The b_2 is positive on the west side, and in particular, is more positive toward the west and south. It is negative for the east side and becomes increasingly negative toward the east and south. The zero contour (the white area and the green curve) is along the 85°W to 95°W longitude line (notice that b_2 has a $3° \times 3°$ spatial resolution) and is slightly tilted westward in azimuth. The 85°W to 95°W line defines longitudes of least temporal variability for this mode, since the TEC component for this mode $T_2 = b_2(\phi, \lambda) P_2(t, n)$ and T_2 will stay zero if b_2 is zero, regardless of temporal variability in P_2. A very small portion of these longitudes were previously examined in *Zhang et al.* [2011] where three midlatitude zones in the continental U.S. were examined based on morning-to-evening variability derived from a month-long TEC data set. In this study, application of the EOF technique allows us to precisely define the full extent of these longitudes using the entire 12 year long data set. Significantly, our analysis reveals that these longitudes happen to be along zero magnetic declination in North America as shown by the black line, strongly suggesting an important correlation between T_2 and declination.

3.2. Temporal Variations $P_2(t, n)$

[12] The principal component for the second mode, $P_2(t, n)$, describes temporal variability in the T_2 component (Figure 3). The color-shaded variation in Figure 3a representing the whole $P_2(t, n)$ data set shows a well-defined dependence on local time and on month and year. The monthly variation, $p_2(n)$ (diurnally averaged), fluctuates about an overall negative average (the horizontal gray line) with substantial monthly (red line) and yearly (black line) variability. The yearly variation seems to be somewhat correlated with the solar 10.7 cm flux index F10.7, in particular, its yearly averages (Figure 3b). In fact, $P_2(t, n)$ can be further decomposed into a new EOF basis $\beta_j(t, m)$, representing monthly (m) and diurnal (t) variations, and a new principal component $\rho_j(y)$, representing yearly (y) variations, i.e., $P_2(t, n) = \sum_j \beta_j(t, m) \rho_j(y)$. The first mode, $\rho_1(y)$ (line and circles in Figure 3b), is highly correlated with F10.7: High solar activity corresponds to a large $P_2(t, n)$ magnitude.

[13] Therefore inserting $P_2(t, n)$ and $b_2(\phi, \lambda)$ information into the TEC component T_2, we conclude that (1) on average, T_2 is positive on the east side and negative on the west side,

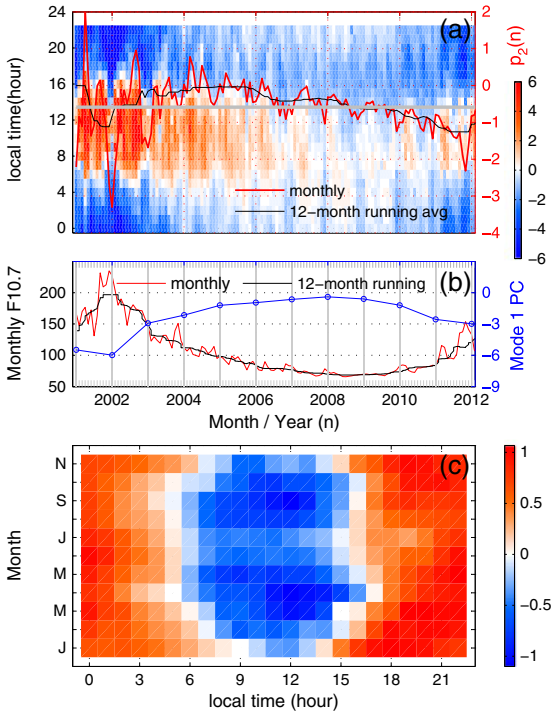

Figure 3. (a) The second EOF mode principal component $P_2(t, n)$, shown as coded colors as a function of local time and month/year, overlapped with (using the y axis on the right) monthly average $p_2(n)$ (averaging over local times) and its 12 month running average. The horizontal gray line is the level of the gross average for $P_2(t, n)$. (b) Anticorrelation between F10.7 index (red line for monthly and black line for 12 month running averages) and intensity of $P_2(t, n)$ (blue line and circles), derived as the first EOF mode principal component for $P_2(t, n)$ (see text). (c) Seasonal and local time variations of $P_2(t, n)$, derived as the first EOF mode basis for $P_2(t, n)$ (see text).

i.e., TEC tends to be higher to the east than to the west. (2) East-west differences, as presented in this EOF mode, appear to be positively correlated with solar activity, being strong at solar maximum and weak at solar minimum.

[14] There are substantial day-night and summer-winter differences in $P_2(t,n)$. These were shown in Figure 3a and are further illustrated in the first mode $\beta_1(t,m)$ (Figure 3c), which is a decomposed local time versus month basis function for $P_2(t,n)$. This basis function is negative, and therefore, $P_2(t,n)$ is positive due to negative $\rho_1(y)$ approximately between 8 daytime hours 06:00–14:00 LT and positive for the better part of the day. As a result of this day-night asymmetry, $P_2(t,n)$ is biased toward negative values (see the horizontal line in Figure 2b as well), and therefore, the TEC component T_2 is positive (higher TEC) on the east side at night and on the west side during the day.

[15] The local time dependency in $\beta_1(t,m)$ is modulated by seasonal variability both in duration for being positive or negative and in magnitude. The $\beta_1(t,m)$ shows maximum magnitudes in equinox months for 8 h during the day and maximum magnitudes in winter for all other local times. Accordingly, east-west differences in TEC, represented by T_2, are largest at winter night and by equinox day.

3.3. Coincident Spatial Variations in b_2 and Wind Dynamics

[16] The substantial TEC control enforced by Earth's magnetic fields, in particular the declination D and dip angle I, is particularly evident when examining overlapping contours of $v^z_\perp = 200 \cos I \sin I \sin D$ in Figure 2. This $v^z_\perp$ expression assumes 200 m/s thermospheric westward winds that induce vertical ion drifts, upward for D positive (the west side), and downward for D negative (the east side). Thermospheric winds are highly variable in space and time. The 200 m/s wind is typical for the midlatitude F region ionosphere at night, but of course, assumption on this wind constant affects the wind effect efficiency but does not affect spatial variations in $v^z_\perp$. In the longitude/latitude sector under study, the latitude varies by ~40° and the longitude by ~90°, I varies between 34°–83°, and D varies between –27° to +21°. We find therefore that the directional reverse across zero declination and dynamical forcing represented by $v^z_\perp$ contours match well with the spatial symmetry in the second EOF mode of TEC variations.

3.4. Relative Significance of the Second EOF Mode

[17] The significance of the second EOF mode may be assessed by different measures: T_2 variance = 1.57, accounting for 1.61% of the total variance (for comparison, the first mode T_1 variance = 91.9, accounting for 94.0% of the total variance) and the third mode T_3 variance = 1.24, accounting for 1.27% of the total variance. We note that some well-known midlatitude phenomena, such as daytime electron density levels being higher in winter than in summer [*Rishbeth*, 1998], are observed in the third mode, but apparently are not as significant as longitudinal variations represented in the second EOF mode. This effect will be the subject of a future study.

4. Discussion and Conclusion

[18] The second EOF mode of TEC data exhibits strong longitudinal variations that retain significant variability in local time, season, and to a lesser extent, solar activity. These longitudinal variations are essentially symmetric around the zero magnetic declination line. Results shown in Figure 2 clearly demonstrate a smooth and gradual longitudinal progression and reveal the large extension of this symmetry into both higher and lower midlatitudes. These results also reveal a pronounced similarity between the longitudinal and latitudinal pattern in b_2 and in the zonal wind induced vertical drift $v^z_\perp$. This strongly suggests a causative zonal wind effect on ionospheric variations, as proposed by *Zhang et al.* [2011], but our study quantifies for the first time the large spatial extent and significant amplitude of its effect. For a westward thermospheric wind, $v^z_\perp$ is upward on the west side and downward on the east side due to opposite declination angles and therefore drives east-west differences in electron densities since chemical recombination rates fall off exponentially with height. While longitudinal variation is clearly a dominant characteristic, there appears minor latitudinal variation, in particular, at lower latitudes on the west side where b_2 does not perfectly match $v^z_\perp$. This variation is originated more likely from low-latitude electrodynamics than midlatitude wind-declination dynamics.

[19] Temporal variability in T_2, as a function of solar activity, season, and local time, reflects well similar patterns in zonal wind climatology. These effects were demonstrated in *Zhang et al.* [2012b] based on winds and electron density measurements over Millstone Hill in the northeast U.S. Derived from a much larger region, our results suggest that in order to explain the $P_2(t,n)$ variability, (1) the zonal winds at winter night and by equinox day must be the strongest, (2) the daytime zonal wind must be mostly westward and the nighttime one eastward, and (3) the zonal wind may be dependent on solar cycle. These zonal wind characteristics over North America generally agree with known wind climatology, e.g., in empirical models [*Drob et al.*, 2008]. The solar cycle dependence in (3), in particular, is somewhat complicated since prior observations show increasing wind speeds with either decreasing [*Zhang et al.*, 2012a] or increasing solar activity [*Brum et al.*, 2012], depending on many factors [*Emmert et al.*, 2006]. These factors control the relative importance of competing forces such as neutral pressure gradients and ion drag.

[20] In midlatitude ionospheric dynamics, meridional winds (u_m) play significant roles by inducing vertical drifts $v^m_\perp = u_m \cos I \sin I \cos D$, where the $\cos D$ factor varies primarily between 0.9 and 1. In Figure 1a, contours of $v^m_\perp$ for u_m = 200 m/s are given as dashed lines. The $v^m_\perp$ appears to follow CGM (Corrected GeoMagnetic) latitude (white solid lines) closely. We therefore conclude that spatially uniform meridional winds at a given local time can only cause the type of TEC variations in Figure 1a, patterns representing a gross average of the monthly means as shown in the first EOF mode.

[21] Longitudinal homogeneity of winds for a given local time, however, remains an open question. Neutral pressure gradients and horizontal viscosity may contribute to maintaining longitudinal homogeneity of winds for a given local time, while other localized factors such as ion drag on neutral particles or wave forcing [*Lühr et al.*, 2007] may serve as a potential contributor to the inhomogeneity. So far, however, there is no indication of longitudinal changes in meridional winds, which would vary as a function of local time and season, that could systematically explain observed

longitudinal changes in T_2 at midlatitudes during nonstorm conditions. TIE-GCM simulations of *magnetic* meridional winds do show some longitudinal dependency, mostly at midnight [*Luan et al.*, 2008]. These variations are due to the combined declination and zonal wind effect discussed in this study: Longitudinal gradients in geographic meridional winds are much smaller than in magnetic meridional winds. Longitudinal inhomogeneity in zonal winds at given local times has been previously reported primarily at equatorial zones [*Meriwether et al.*, 1997; *Lühr et al.*, 2007] but has rarely been reported at midlatitudes probably due to lack of observations. To this end, future measurements with sufficient high spatial and temporal resolutions as described in *Makela et al.* [2012] will be extremely helpful.

[22] In conclusion, using a 12 year long ground-based GPS TEC data set for North America and performing EOF decomposition for spatial and temporal variations, this paper reveals a large and significant symmetric longitudinal variation of the ionosphere, organized with respect to magnetic declination. The correlation of such a gradual spatial variation to that in zonal wind-driven vertical drifts, along with well-organized temporal variations, strongly suggests a causative mechanism involving varying declination with longitude and varying zonal wind climatology with local time, season, and solar cycle. This study highlights the substantial influence of the geomagnetic field on mesoscale ionospheric structures at midlatitudes.

[23] **Acknowledgments.** We thank the members of the MIT Haystack Observatory for maintaining the Madrigal Database. Observations and research are supported by the US National Science Foundation under grants ATM-0733510, ATM-0856093, and AGS-1242204. Z.C. acknowledges supports from the China Scholarship Council and MIT Haystack Observatory during her stay at Haystack as a visiting student.

[24] The Editor thanks an anonymous reviewer and Biqiang Zhao for their assistance in evaluating this manuscript.

References

A, E., D. Zhang, A. J. Ridley, Z. Xiao, and Y. Hao (2012), A global model: Empirical orthogonal function analysis of total electron content 1999–2009 data, *J. Geophys. Res.*, *117*, A03328, doi:10.1029/2011JA017238.

Brum, C. G. M., C. A. Tepley, J. T. Fentzke, E. Robles, P. T. dos Santos, and S. A. Gonzalez (2012), Long-term changes in the thermospheric neutral winds over Arecibo: Climatology based on over three decades of Fabry-Perot observations, *J. Geophys. Res.*, *117*, A00H14, doi:10.1029/2011JA016458.

Coster, A. J., J. C. Foster, and P. J. Erickson (2003), Monitoring the ionosphere with GPS, *GPS World*, *14*(5), 42–45.

de Larquier, S., J. M. Ruohoniemi, J. B. H. Baker, N. Ravindran Varrier, and M. Lester (2011), First observations of the midlatitude evening anomaly using Super Dual Auroral Radar Network (SuperDARN) radars, *J. Geophys. Res.*, *116*, A10321, doi:10.1029/2011JA016787.

Daniell Jr., R. E., L. D. Brown, D. N. Anderson, M. W. Fox, P. H. Doherty, D. T. Decker, J. J. Sojka, and R. W. Schunk (1995), Parameterized ionospheric model: A global ionospheric parameterization based on first principles models, *Radio Sci.*, *30*(5), 1499–1510, doi:10.1029/95RS01826.

Drob, D. P. et al. (2008), An empirical model of the Earth's horizontal wind fields: HWM07, *J. Geophys. Res.*, *113*, A12304, doi:10.1029/2008JA013668.

Emmert, J. T., M. L. Faivre, G. Hernandez, M. J. Jarvis, J. W. Meriwether, R. J. Niciejewski, D. P. Sipler, and C. A. Tepley (2006), Climatologies of nighttime upper thermospheric winds measured by ground-based Fabry-Perot interferometers during geomagnetically quiet conditions: 1. Local time, latitudinal, seasonal, and solar cycle dependence, *J. Geophys. Res.*, *111*, A12302, doi:10.1029/2006JA011948.

Eyfrig, R. W. (1963), The effect of the magnetic declination on the F 2 layer, *J. Geophys. Res.*, *68*(9), 2529–2530, doi:10.1029/JZ068i009p02529.

Goldberg, R. A. (1966), A theoretical model for the magnetic declination effect in the ionospheric F region, *Ann. Geophys.*, *22*, 588–598.

He, M., L. Liu, W. Wan, and B. Zhao (2011), A study on the nighttime midlatitude ionospheric trough, *J. Geophys. Res.*, *116*, A05315, doi:10.1029/2010JA016252.

Kil, H., R. De Majistre, L. J. Paxton, and Y. Zhang (2006), Nighttime-region morphology in the low and middle latitudes seen from DMSP F15 and TIMED/GUVI, *J. Atmos. Sol. Terr. Phys.*, *68*, 1672–1681.

Kohl, H., J. W. King, and D. Eccles (1969), An explanation of the magnetic declination effect in the ionospheric F2-layer, *J. Atmos. Terr. Phys.*, *31*(7), 1011–1016.

Lei, J., T. Matsuo, X. Dou, E. Sutton, and X. Luan (2012), Annual and semiannual variations of thermospheric density: EOF analysis of CHAMP and GRACE data, *J. Geophys. Res.*, *117*, A01310, doi:10.1029/2011JA017324.

Lin, C. H., C. H. Liu, J. Y. Liu, C. H. Chen, A. G. Burns, and W. Wang (2010), Midlatitude summer nighttime anomaly of the ionospheric electron density observed by FORMOSAT-3/COSMIC, *J. Geophys. Res.*, *115*, A03308, doi:10.1029/2009JA014084.

Lühr, H., K. Husler, and C. Stolle (2007), Longitudinal variation of F region electron density and thermospheric zonal wind caused by atmospheric tides, *Geophys. Res. Lett.*, *34*, L16102, doi:10.1029/2007GL030639.

Luan, X., W. Wang, A. Burns, S. C. Solomon, and J. Lei (2008), Midlatitude nighttime enhancement in F region electron density from global COSMIC measurements under solar minimum winter condition, *J. Geophys. Res.*, *113*, A09319, doi:10.1029/2008JA013063.

Makela, J. J., J. W. Meriwether, A. J. Ridley, M. Ciocca, and M. W. Castellez (2012), Large-scale measurements of thermospheric dynamics with a multisite Fabry-Perot interferometer network: Overview of plans and results from midlatitude measurements, *International J. Geophys.*, *2012*, 1–10, Article ID 872140, doi:10.1155/2012/87214.

Mannucci, A. J., B. D. Wilson, D. N. Yuan, C. H. Ho, U. J. Lindqwister, and T. F. Runge (1998), A global mapping technique for GPS-derived ionospheric total electron content measurements, *Radio Sci.*, *33*(3), 565–582.

Matsuo, T., A. D. Richmond, and D. W. Nychka (2002), Modes of high-latitude electric field variability derived from DE-2 measurements: Empirical Orthogonal Function (EOF) analysis, *Geophys. Res. Lett.*, *29*(7), 1107, doi:10.1029/2001GL014077.

Meriwether, J. W., M. A. Biondi, F. A. Herrero, C. G. Fesen, and D. C. Hallenback (1997), Optical interferometric studies of the nighttime equatorial thermosphere: Enhanced temperatures and zonal wind gradients, *J. Geophys. Res.*, *102*(A9), 20041–20058, doi:10.1029/97JA01463.

Orus, R., M. Hernandez-Pajares, J. M. Juan, and J. Sanz (2005), Improvement of global ionospheric VTEC maps by using kriging interpolation technique, *J. Atmos. Sol. Terr. Phys.*, *67*(16), 1598–1609.

Qian, L., A. G. Burns, S. C. Solomon, and W. Wang (2013), Annual/semiannual variation of the ionosphere, *Geophys. Res. Lett.*, *40*, 1928–1933, doi:10.1002/grl.50448.

Rideout, W., and A. Coster (2006), Automated GPS processing for global total electron content data, *GPS Solut.*, *10*, 219-228, doi:10.1007/s10291-006-0029-5.

Rishbeth, H. (1998), How the thermospheric circulation affects the ionospheric F2-layer, *J. Atmos. Sol-Terr. Phys.*, *60*, 1385–1402.

Wilson, B. D., C. H. Yinger, W. A. Fees, and C. Shank (1999), New and improved: The broadcast interfrequency biases, *GPS World*, *10*(9), 56–66.

Xu, J. S., X. J. Li, Y. W. Liu, and M. Jing (2013), TEC differences for the mid-latitude ionosphere in both sides of the longitudes with zero declination, *Adv. Space Res.*, [online] Available from: http://www.sciencedirect.com/science/article/pii/S027311771300029X.

Zeng, Z., A. G. Burns, W. Wang, J. Lei, S. C. Solomon, S. Syndergaard, L. Qian, and Y.-H. Kuo (2008), Ionospheric annual asymmetry observed by the COSMIC radio occultation measurements and simulated by the TIEGCM, *J. Geophys. Res.*, *113*, A07305, doi:10.1029/2007JA012897.

Zhang, S.-R., J. C. Foster, A. J. Coster, and P. J. Erickson (2011), East-West Coast differences in total electron content over the continental US, *Geophys. Res. Lett.*, *38*, L19101, doi:10.1029/2011GL049116.

Zhang, S.-R., A. J. Coster, J. M. Holt, J. C. Foster, and P. J. Erickson (2012a), Ionospheric longitudinal variations at midlatitudes: Incoherent scatter radar observation at Millstone Hill, *Sci. China Technol. Sci.*, *55*(5), 1153–1160, doi:10.1007/s11431-012-4784-y.

Zhang, S.-R., J. C. Foster, J. M. Holt, P. J. Erickson, and A. J. Coster (2012b), Magnetic declination and zonal wind effects on longitudinal differences of ionospheric electron density at midlatitudes, *J. Geophys. Res.*, *117*, A08329, doi:10.1029/2012JA017954.

Zhao, B., W. Wan, L. Liu, X. Yue, and S. Venkatraman (2005), Statistical characteristics of the total ion density in the topside ionosphere during the period 1996–2004 using empirical orthogonal function (EOF) analysis, *Ann. Geophys.*, *23*, 3615–3631, doi:10.5194/angeo-23-3615-2005.

Zhao, B., M. Wang, Y. Wang, Z. Ren, X. Yue, J. Zhu, W. Wan, B. Ning, J. Liu, and B. Xiong (2013), East-west differences in F-region electron density at midlatitude: Evidence from the far east region, *J. Geophys. Res. Space Physics*, *118*, 542–553, doi:10.1029/2012JA018235.